4-24-2012 12:00 AM

A Method to Measure the Detective Quantum Efficiency of Radiographic Systems in Clinical Setting

Michael C. McDonald
The University of Western Ontario

Supervisor
Dr. Ian Cunningham
The University of Western Ontario

Graduate Program in Biomedical Engineering
A thesis submitted in partial fulfillment of the requirements for the degree in Master of Engineering Science

A METHOD TO MEASURE THE DETECTIVE QUANTUM EFFICIENCY OF RADIOGRAPHIC SYSTEMS IN A CLINICAL SETTING

(Spine title: A Method to Measure the Detective Quantum Efficiency of Radiographic Systems in a Clinical Setting)

(Thesis format: Integrated Article)

by

Michael McDonald

Graduate Program in Biomedical Engineering

A thesis submitted in partial fulfillment
of the requirements for the degree of
Masters of Engineering Science

The School of Graduate and Postdoctoral Studies
The University of Western Ontario
London, Ontario, Canada

THE UNIVERSITY OF WESTERN ONTARIO
School of Graduate and Postdoctoral Studies

CERTIFICATE OF EXAMINATION

Supervisor:

.....
Dr. I. A. Cunningham

Joint Supervisor:

.....
N/A

Supervisory Committee:

.....
Dr. D. Holdsworth

.....
Dr. G. Parraga

Examiners:

.....
Dr. T. Peters

.....
Dr. J. Lacefield

.....
Dr. E. Wong

The thesis by

Michael McDonald

entitled:

A Method to Measure the Detective Quantum Efficiency of Radiographic Systems in a Clinical Setting

is accepted in partial fulfillment of the
requirements for the degree of
Masters of Engineering Science

.....
Date

.....
Chair of the Thesis Examination Board

Abstract

The risks associated with exposure to radiation make it critical that digital-imaging systems give the best possible images for a given dose to the patient. The DQE is the most widely accepted measure of performance and dose efficiency for digital radiography systems, however it is not commonly measured in a clinical environment as part of routine quality assurance. The primary reason for this is that the data provided to the user by clinical systems has typically undergone image-processing and therefore may have a non-linear characteristic response. In this thesis a method to measure the DQE using processed image data is presented using a novel theoretical approach to the linearization of the system characteristic response. The method was validated on cesium iodide-based digital radiography flat panel detector and the results where within a few percent of a conventional DQE measurement.

Keywords: x ray, quality assurance, detective quantum efficiency, digital radiography, performance, linear-systems theory, small-signal, noise, modulation transfer function, non-linear

Co-Authorship

This thesis contains material from a manuscript to be submitted for publication. I was responsible for theoretical development, collection of experimental data, analysis and interpretation of data, and preparation of the manuscript. These tasks where performed under the supervision and guidance of I.A. Cunningham, who assisted with theoretical development and edited the manuscript. H.Y. Kim contributed ideas to the theoretical development.

Acknowledgments

I would like to acknowledge the support of the following people who helped me on the way to successfully completing this thesis.

- My supervisor: Dr. Ian Cunningham. This project would have been impossible without the guidance he provided. Although he was sometimes hard on me, I am better for it.

- My advisory committee: Dr. Grace Parraga, Dr. David Holdsworth. for their helpful advice and suggestions.

- Other collaborators: John Henry of the London Health Sciences Center for assistance with equipment and experiments. Prof. Ho-Kyung Kim of Pusan National University, South Korea for his helpful insights and discussions.

- My lab colleagues Jesse Tanguay, Christian Dihel and Seugmen Yeun, for camaraderie and support.

Contents

List of Tables

List of Figures

LIST OF ABBREVIATIONS AND ACRONYMS

ALARA	As Low As Reasonably Achievable
AAPM	American Association of Physicists in Medicine
BaFX:Eu	europium activated barium fluorohalide
cm	centimeter
CR	computed radiography
CsI	cesium iodide
DQE	detective quantum efficiency
DR	digital radiography
Eq.	Equation
Fig.	Figure
g	gram
Gd_20_2S	gadolinium oxysulde
Gy	Gray
HVL	half-value layer
IEC	International Electrotechnical Commission
IPEM	Institute of Physics and Engineering in Medicine
J	Joule
keV	kiloelectron volt
kg	kilogram
LSS	linearized small-signal

mm	millimeter
mR	milliRoengton
mSv	milliSievert
MTF	modulation transfer function
NEMA	National Electrical Manufactures Association
NEQ	noise-equivalent quanta
NIST	National Institute of Standards and Technology
NPS	Weiner noise power spectrum
PSF	point-spread function
QA	quality assurance
QE	quantum efficiency
R	Roengton
ROI	region of interest
SNR	sign-to-noise ratio
Sv	Sievert
TFT	thin-film transistor
UK	United Kingdom

LIST OF SYMBOLS

Symbol	Units	Description
$\alpha(E)$	-	detector quantum efficiency
a	mm^2	pixel area
α	-	quantum efficiency
β	-	edge-attenuation factor
$\bar{d_s}$	-	non-glare pixel value component
$\bar{d_g}$	-	glare pixel value component
$\bar{d_e}$	-	contribution to pixel value from scatter
$\bar{d_p}$	-	contribution to pixel value of the primary transmitted x ray
$\overline{d}$	-	pixel value
$\bar{d}_{\mathrm{L}}$	-	linearized pixel value
$\triangle d$	-	$d - \bar{d}$
DQE()	-	detective quantum efficiency
E	keV	photon energy
E_d	keV	x-ray energy deposited in the pixel
$\hat{E}$	keV mm^{-2}	area density of deposited energy
E_q	keV	average energy deposited per incident x-ray photon
$E_a(E)$	keV	average x-ray energy deposited in the detector by a photon having energy E

Symbol	Units	Description
$f()$	-	system characteristic function
f_q^{-1}	-	linearizing transformation
G	mm^2	system gain
G_s	mm^2	gain determined using the LSS method
G_g	mm^2	gain component due to glare
k_{L}	-	constant of proportionality
k	-	constant of proportionality
$K()$	mm^2	two dimensional auto-covariance function
$\bar{N}$		average number of detector incident quanta
NEQ()	mm^{-2}	noise-equivalent quanta
$NPS()$	mm^2	Weiner noise power spectrum
ρ	$\mathrm{g\ cm}^{-3}$	density
$\overline{q}$	mm^{-2}	quanta per unit area incident on the detector
Q_o	$\mathrm{mm}^2/\mathrm{mR}$	number of x ray quanta in the beam per unit exposure
$s(E)$	-	normalized x ray spectrum
$S(u)$	-	normalized scatter point-spread function
SNR		signal-to-noise ratio
$\mathrm{T_S}(u)$	-	MTF measured using the semi-transparent edge method
$\mathrm{T_L}(u)$	-	linearized small-signal MTF
T()	-	modulation tranfer function

Symbol	Units	Description
$\mathrm{T}(,)$	-	two-dimensional system transfer function
t	cm	attenuator thickness
τ_y	mm	distance between two points in x
τ_x	mm	distance between two points in y
$\mu()$	cm^{-1}	linear attenuation coefficient
u	mm^{-1}	spatial frequency
u	mm^{-1}	spatial frequency corresponding to x
v	mm^{-1}	spatial frequency corresponding to y
γ	-	edge-scatter-to-primary ratio
$\mathrm{W}(u)$	mm^2	image Wiener NPS
$\mathrm{W}_{\bar{q}}(u)$	mm^{-2}	Wiener NPS of the incident Poisson-distributed quanta
$\mathrm{W}_L(u)$	mm^2	linearized small-signal Wiener NPS
X	mR	exposure incident on the detector
x	-	system input
y	-	system output

Chapter 1

Introduction

X-ray imaging is an invaluable tool to medical practitioners in the assessment of disease and injury. Today, x-ray radiography (and related x-ray based methods including computed tomography, fluoroscopy and mammography) are collectively the most widely used modalities for medical imaging with 138 million x-ray procedures performed globally every year [1]. While medical imaging provides a non-invasive way of examining internal anatomy, x rays are a form of ionizing radiation and therefore are believed to present a carcinogenic risk to the patient [2].

Given these risks of x-ray exposure, it is essential that the benefits to the patient of the imaging procedure outweigh the costs in terms of biological risk. The principle of ALARA (As Low As Reasonably Achievable) is observed for imaging procedures [3] and requires that patient equivalent dose be minimized as much as possible without compromising necessary diagnostic benefits of the examination. Although it is desireable to keep patient exposures as low as possible to minimize risks from exposure to radiation, the statistical nature of x-ray interactions results in image noise when too few x-ray photons are used to create the image. This has been understood since the pioneering work of Albert Rose [4, 5] and others, and means there is a fundamental trade-off between patient dose (number of quanta) and image quality. To achieve an

optimal balance, it is critical that x-ray detectors be designed and maintained to produce the best possible image quality for a given radiation exposure. Unfortunately, not all x-ray systems provide patients with the benefits of optimal image quality for a given exposure, particularly for the visualization of small structures and fine detail.

A metric called the detective quantum efficiency (DQE) describes how close a detector is to the optimal balance of image quality and exposure. While the DQE is widely accepted by scientific communities [6], it is until now been difficult or impossible to measure in a clinical envirnoment. Thus, while regulatory agencies (in Ontario this is the Healing Arts Radiation Protection Act) mandate allowable patient exposures for standard examinations, we do not know whether we are getting the best possible images for these exposures. We believe the only way of ensuring optimal image quality and low patient exposures in medical radiography is to measure the DQE of clinical imaging equipment as part of routine quality assurance testing, so that corrective action can be taken when indicated. The objective of this research is to develop a method of measuring the DQE that can be implemented in a clinical environment.

1.1 Biological Effects of Ionizing Radiation

X-ray photons interact with matter by one of several physical mechanisms. In the diagnostic energy range (approximately 20 to 120 keV) these are photoelectric interactions, incoherent (Compton) scatter and coherent (elastic) scatter. For medical imaging purposes, a very important contrast forming interaction is the photoelectric mechanism in which an inner-shell electron atom is liberated by an incoming x-ray photon of sufficient energy [7], causing the emmission of a characteristic x-ray. For soft tissues, these characteristic emmissions have a low energy and are readily absorbed by nearby tissues. The liberated electrons will impart their kinetic energy to

the surrounding medium, producing free radicals with subsequent carcinogenic and hereditary effects [8].

The concept of absorbed dose is used to quantify how much energy is imparted to the medium by ionizing radiation and is measured in Joules per kilogram [J/kg], with units of Gray (Gy). Different types of of ionizing radiation have different effects, and therefore the concept of equivalent dose is used to quantify the biological risk associated with a particular type of radiation and is measured in Sieverts [Sv]. The equivalent dose is defined as the absorbed dose multiplied by a quality factor that weights the biological effectiveness of the radiation type (for x-rays the quality factor is unity).

X-ray imaging procedures are typically targeted to a specific area of the body where the biological effects of ionizing radiation vary depending on the type and volume of tissue being irradiated. The concept of effective dose is used to determine the equivalent dose to a uniformly exposed body that has the same biological risk as a non-uniform exposure of a particular area. It is calculated as the equivalent dose multiplied by a quality factor that weights the relative biological risks for the type of tissue. For instance, a dose of 70 mSv (typical for a chest CT [9]) to the lungs has a weighting factor of 0.12 [3], and therefore has a whole body effective dose of 8 mSv. It has been found that the lifetime risk of fatal cancer varies between approximately 3% and 5% per Sievert depending on the individuals' age and the pattern of exposure [10].

1.2 X-Ray Detectors

Although there are a great number of technologies for the detection of x rays, the focus of this work is principally with application to digital systems used for diagnostic radiography. Discussions of other methods of x-ray detection, such as film-screen

technologies, will be omitted.

X-ray detectors in general radiography can be classified in two categories: direct and indirect detection systems. In direct detectors, x-ray interactions occur in a photoconductive layer (typically selenium) that is sandwiched between two electrodes and biased at high voltage. X-ray interactions in the selenium cause charge to be released which migrates to the electrodes where the total accumulation is measured [7].

In indirect detectors, a scintillating layer is employed that converts interacting x rays to optical photons and couples them to a thin-film transistor (TFT) array. Commonly used materials for the scintillator are gadolinium oxysulfide (Gd_20_2S) for unstructured types and cesium iodide (CsI) based for structured scintillators. A subtype of these indirect detectors are the photostimulable phosphor detectors which is the technology employed in modern computed radiography (CR) systems. Typically, a plate containing a layer of (most commonly) barium fluorohalide activated with europium ions (BaFX:Eu) [11] is exposed to x rays causing energy to be stored in excited electrons. The plate is then stimulated by a laser that causes release of energy and emission of visible light [12].

In both direct and indirect systems, x rays interact imparting energy to the detector material. Therefore the output "signal" of a detector is proportional to the total energy deposited in the detector element over the period of time in which the x-ray exposure is in progress [13]. Because of this, these detectors are sometimes called "energy integrating" detectors.

1.3 X-Ray Detector Performance

The different x-ray imaging systems in use each have different advantages and disadvantages. An understanding of the merits of each system requires an objective metric

of image quality and detector performance. For digital radiography, the two primary considerations are dose to the patient and image quality [14]. The detective quantum efficiency (DQE) is the most widely accepted metric that encapsulates these two considerations [6]. It is an objective measure of detector performance and describes, on an abolute scale, the "dose efficiency" of the detector relative to a carefully defined ideal. In this section, the concepts of image quality, dose, and DQE are presented.

1.3.1 Image Quality and Dose

Image quality in x-ray imaging is ultimately dependant on the signal-to-noise ratio (SNR) [15]. Due to the nature of the way x rays are produced and arrive at the detector, that is, by the random emission of x ray photons from the source and subsequent detection according to Poisson statistics, the x-ray beam itself can be thought of as having an intrinsic signal-to-noise ratio given by SNR $= \bar{N}/\sigma_N = \sqrt{\bar{N}}$, where $\bar{N}$ is the average number of incident photons and $\sigma_N = \sqrt{\bar{N}}$ for a Poisson random variable. The statistical variation in the number of detected quanta is known as "quantum noise" and imposes a fundamental upper limit of signal-to-noise ratio, and therefore image quality, that can be achieved with the detector. A greater number of quanta results in higher SNR, but generally at a higher dose. This is the fundamental trade-off between radiation dose and x-ray image quality.

1.3.2 Quantum Efficiency

The SNR will be degraded if not all incident x-ray photons interact in the detector. The quantum efficiency (QE) is the fraction of photons in the incident x-ray beam that interact in the detector materials [16], and is therefore the probability that photons will interact in the detector and an important metric of performance. For a CsI-based detector exposed to a standardized RQA-5 (70kV, 21mm Al) spectrum [17] and a 0.5-mm thick layer of CsI, this value is approximately 0.53 [18]. The QE can be

increased by increasing the thicknesses of the detection layer. However, this must be balanced with numerous other design considerations such as system resolution which generally degrades as detector thickness increases [19]. While one might expect those detectors with the highest QE to produce images with the highest SNR for a given dose, reality is generally more complex.

1.3.3 Detective Quantum Efficiency

In practice, other physical processes in the detector may reduce the SNR futher. The concept of detective quantum efficiency (DQE) is used to describe SNR in terms of an *effective* or *equivalent* quantum efficiency. The idea originated in the early work of Shaw[20] and is an extension of the work of Albert Rose [4, 5]. The "equivalent quantum efficiency" described by Shaw [20], now called the detective quantum efficiency, is the effective fraction of x-ray quanta contributing to image signal-to-noise, and thus is analogous to the QE but takes in to account additional noise introduced by the detector. The DQE is properly considered as a function of spatial frequency. However, in order to faciliate an understanding of the concept, it is helpfull to first consider a simplified "particle-based" explanation of the DQE.

Consider a hypothetical ideal detector that introduces no noise of its own. For this detector the output signal is directly proportional to the number of (mono-energetic) quanta that interact in the detector:

$$\bar{d} = k\alpha\bar{N}, \tag{1.1}$$

where $\bar{d}$ is the detector signal (typically a digital value), k is a constant of proportionality, and α is the QE of the detector. Noise is defined as the statisitcal fluctuations in the detector signal. For an amplification process by the binary random variable α [21]:

$$\sigma_{\bar{d}}^2 = k^2 \left[\alpha^2 \sigma_{\bar{N}}^2 + \bar{N}\sigma_{\alpha}^2\right] = k^2 \alpha \bar{N}. \tag{1.2}$$

The detector signal-to-noise ratio (SNR) is therefore given by:

$$\mathrm{SNR_d} = \frac{\bar{d}}{\sigma_{\bar{d}}} = \frac{k\alpha\bar{N}}{k\sqrt{\alpha\bar{N}}} = \sqrt{\alpha\bar{N}}. \tag{1.3}$$

Images are generally scaled by an arbitrary factor for display, and hence absolute signal values have little meaning. To address this problem, the concept of the noise equivalent quanta (NEQ) [20] was developed to express image SNR in terms of a number of Poisson distributed quanta interacting in an ideal detector that gives the same SNR as is actually observed. For the ideal system considered here, this is equal to the number of interacting quanta:

$$\mathrm{NEQ} = \alpha\bar{N} = \mathrm{SNR_d^2}. \tag{1.4}$$

For a real detector, the NEQ is generally less than $\alpha\bar{N}$ due to noise added by the detector, such as amplifier electronic noise. The ratio of NEQ to the number of incident quanta is the DQE and is a measure of detector performance to capture the fundamental SNR of the beam. For the ideal system, the DQE is expressed as:

$$\mathrm{DQE} = \frac{\mathrm{NEQ}}{\bar{N}} = \alpha. \tag{1.5}$$

While the NEQ describes image quality, the DQE is a measure of system performance. The DQE will never exceed the system QE, and will be less for a non-ideal system. The DQE is therefore a measure of "image quality per incident x-ray quantum" and is therefore a surrogate measure of the system's dose efficiency.

The simple description of DQE detailed in this section is helpfull to the understanding of the concept. However, it assumes that noise in the detector is spatially

uncorrelated, an assumption that breaks down in real imaging systems where physical processes can introduce statistical correlations in image signals from the scatter of x rays, secondary image quanta in the detector system, and possibly electronic noise [22]. These factors have the effect of altering the visual texture of noise, which affects what can be seen in an image [23], without necessarily affecting the variance measurement. It is therefore necessary to specify the DQE in a way that quantifies the statistical correlations that may exist. To do this requires the use of Fourier transform [24] based metrics, specifically the concepts of noise power spectrum (NPS) and modulation transfer function (MTF). Both of these concepts emerge from an area of mathematics known as linear systems analysis.

1.3.4 Linear Systems Analysis

To be amenable to Fourier analysis, a system must have a linear characteristic response [25]. That is, the system output quantity must be proportional to the system input quantity. In x-ray imaging, that requires

$$\bar{d} = k\bar{q}, \tag{1.6}$$

where k is a constant of proportionality. In addition, Fourier analysis requires a shift-invariant system, which means that the system point spread function (PSF), which is the impulse response of the system, is independent of the physical location of measurement in the image plane [25].

1.3.5 MTF

The modulation transfer function (MTF), is defined as the modulus of the Fourier transform of the normalized system point-spread function (PSF) [26]:

$$\mathrm{MTF}(u,v) = \left| \mathcal{F}\left\{ \frac{\mathrm{PSF}(x,y)}{\iint \mathrm{PSF}(x,y)\mathrm{d}x\mathrm{d}y} \right\} \right| \tag{1.7}$$

where $\mathcal{F}\{\,\}$ indicates the Fourier transform, $\mathcal{F}\{\mathrm{PSF}(x,y)\}$ is the system two-dimensional transfer function $\mathrm{T}(u,v)$, and by the Fourier central ordinate theorem, $\iint \mathrm{PSF}(x,y)\mathrm{d}x\mathrm{d}y = \mathrm{T}(0,0)$. Thus, the MTF may equivalently be defined as $\mathrm{T}(u,v)$ normalized by $\mathrm{T}(0,0)$. The MTF describes the change in amplitude (scaling) of sinusoidal waveforms passing through an imaging system. For many imaging systems, the MTF contains enough radial symmetry that it is only necessary to express it along the two orthogonal x and y (u and v) directions.

1.3.6 Wiener Noise Power Spectrum

The Wiener noise power spectrum (NPS) [27] is defined as the Fourier transform of the auto-covariance function which describes the statistical correlation of a signal at two image positions separated by a finite distance [28], i.e.

$$\mathrm{NPS}(u,v) = \mathcal{F}\{\mathrm{K}(\tau_x,\tau_y)\} \tag{1.8}$$

where

$$\mathrm{K}(\tau_x,\tau_y) = \lim_{X\to\infty}\lim_{Y\to\infty}\frac{1}{XY}\int_X\int_Y \Delta d(x',\,y')\Delta d(x'+\tau_x,\,y'+\tau_y)\mathrm{d}x'\,\mathrm{d}y' \tag{1.9}$$

is the auto-covariance function, and τ_x and τ_y are the distance between points on the respective axes, and $\Delta d = d - \bar{d}$. In using NPS to characterize noise, it is assumed that the noise processes are wide-sense stationary, that is, the mean value and auto-correlation functions are stationary (shift invariant) across the image. The NPS describes second-order statistics of the image noise and is related to the variance by [29]:

$$\sigma^2 = \iint_{-\infty}^{\infty} \mathrm{NPS}(u,v)\mathrm{d}u\mathrm{d}v. \tag{1.10}$$

The NPS can therefore be viewed as the decomposition of the variance into spatial frequency components.

1.3.7 NEQ and DQE

The noise equivalent quanta, as in the particle based approach, is an expression of image SNR in terms of a number of x ray quanta incident on an ideal system. In the frequency domain, this is expressed as [22]:

$$\mathrm{NEQ}(u,v) = \frac{\bar{q}^2 G^2 \mathrm{MTF}^2(u,v)}{\mathrm{NPS}(u,v)} \tag{1.11}$$

where $\bar{q}$ [mm^{-2}] is the number of quanta per unit area incident on the detector and G [mm^2] is the system gain. The gain is the slope of the system characteristic response which is the ratio of system output (dark-subtracted pixel value $\bar{d}$) to system input, $\bar{q}$, i.e. $G = \bar{d}/\bar{q}$. Therefore,

$$\mathrm{NEQ}(u,v) = \frac{\bar{d}^2 \mathrm{MTF}^2(u,v)}{\mathrm{NPS}(u,v)}. \tag{1.12}$$

The DQE is the effective fraction of input quanta that contribute to image formation:

$$\mathrm{DQE}(u,v) = \frac{\mathrm{NEQ}(u,v)}{\bar{q}} = \frac{\bar{d}^2 \mathrm{MTF}^2(u,v)}{\bar{q}\mathrm{NPS}(u,v)} \tag{1.13}$$

and is therefore an expression of the performance of the system in terms of a ratio of what an image is worth in terms of quality (NEQ) to what it cost in terms of a number of x-ray quanta ($\bar{q}$). The DQE can be determined experimentally by measuring the following three quantities [17, 30]:

1. MTF(u), the one-dimensional (pre-sampling) modulation transfer function in

the x direction using a slanted edge method [31];

2. NPS$(u)/\bar{d}^2$, the one-dimensional Wiener NPS in the x direction normalized by the mean dark-corrected pixel value in images of uniform x-ray exposure; and

3. $\bar{q}$, the mean number of x-ray quanta per unit area incident on the detector.

The importance of the DQE as a primary metric of performance is widely accepted in scientific and regulatory communities. For example, the US Food and Drug Administration (FDA) requires manufacturers to provide MTF and DQE information on new products with 510(k) pre-market notifications.

1.4 Non-Linear Systems and the DQE

Equation 1.13 is the normal expression for the DQE of a linear imaging system. In practice, many systems exhibit a non-linear response due to the result of a deliberate application of image-processing algorithms, electronically manufactured, or inherent to the detector technology that's being employed [32]. In addition, many systems incorporate automatic exposure control and other features that depend on certain patient features or exposure conditions [33]. The result is that processing parameters, and hence the characteristic response of the system, may be adaptive and vary from one exposure to another, and possibly from one region to another in a single image.

An example of a non-linear system in widespread use is computed radiography (CR), which typically has an electronically manufactured logarithmic response in order to mimic film-screen systems. Many modern CR and digital radiography (DR) systems are also non-linear in that they employ image processing where linear data is processed by software to provide features such as window/level adjustments, reverse contrast mapping, histogram equalization, edge enhancement, dynamic range control, and noise control [34]. Seibert [14] described a typical image-processing sequence as

consisting of several distinct steps: In the first step, maximum and minimum values in the image are identified, the image histogram is then shifted and scaled to an appropriate range of brightness and contrast values. This insures that both over- and under-exposed images are mapped to a consistent range of values. Noise suppression is often implemented at this stage by applying spatial smoothing techniques [35] in areas of constant intensity in the image. The next step is the application of non-linear transformations to provide procedure-specific contrast enhancement, or to change the appearance in order to mimic film-screen. The last step is to apply techniques such as unsharp masking [36] in order to enhance the appearance of image edges. This compensates for the inherent detector unsharpness as well as other mechanisms that cause blurring such as finite-focal spot.

Image processing cannot add new information to the image. However, it can increase the diagnostic value of the image by allowing the information that is there to be more readily perceived [37]. In addition, image processing provides a familiar "look" and other improvements to the appearance of the images, however the non-linearity, and in particular non-linear processing which is adaptive to exposure and image conditions makes it difficult or impossible to measure the DQE using conventional methods.

Several investigators have reported DQE measurements for non-linear systems. These studies where limited to either CR systems with an electronically manufactured logarithmic response and image processing disabled, [38, 39, 40, 18] or film/screen systems [41, 42]. The objective of these studies was to measure the DQE of these detectors but not specifically to devise a general method to measure DQE that can be applied to any system, thus the methods used therein are limited in their applicability to those types of systems considered. Stierstorfer and colleagues [43] used small-signal analysis to develop a method with the objective of greater generality, however their method also has certain shortcomings as considered in the following two sections.

1.4.1 Linearization Approach

If the system characteristic response of a system was known for instance as a function of some measurable quantity proportional to deposited energy, such as x-ray exposure, it would be possible to transform measured pixel values to values that are proportional to deposited energy. This effectively linearizes the system response and makes it possible to measure DQE using conventional methods. This idea has been employed successfully in numerous studies of non-linear systems [42, 38, 39, 40, 18, 41]. The technique involves mapping the system output as a function of image plane exposure by variation of x-ray tube output for a fixed spectrum. An obvious requirement for this to be successful is that the response of the system must remain fixed. This can be guaranteed for film/screen systems and CR systems with image-processing disabled. However, many systems implement proprietary image-processing that is not disclosed and cannot be disabled. For these systems this requirement can not be guaranteed.

1.4.2 Small-Signal Approach

Stierestorfer and colleagues [43] described a novel method using small-signal methods to measure the DQE on a wide variety of non-linear systems. In their approach, images of a semi-transparent line pair test pattern are used to measure a form of system modulation. The semi-transparency of the test pattern insures that a globally linear response is not required but rather a behavior that is linear only in the small-signal approximation. The measurement can be made from a single image containing the test pattern and a uniformly exposed area to measure the NPS, circumventing the problem of adaptive processing. This is an impressive accomplishment and it was shown to work on a CR test system, however there are circumstances where this may be ineffective. One problem is that if a system implements edge-enhancement, it will not be possible to get an accurate measurement of the system modulation using the test pattern method. Also problematic is that the magnitude of noise fluctuations

are not always sufficiently small to assume small-signal linearity, thus an error can be incurred in the measurement of the NPS.

Due to the shortcomings noted in the above approaches, the current methods to measure DQE of non-linear systems are not adequate in all situations.

1.5 Quality Assurance and the DQE

Regular quality assurance (QA) is an essential part of proper maintenance and ensuring the system is running at optimal performance. Having adequate quality assurance methods is essential to the performance of many tasks such as constancy testing (monitoring performance over time), acceptance testing (assuring the adequate performance of newly installed equipment), and end of life decision making. Publications by major national bodies: the Association of Physicists in Medicine (AAPM) in the United States, and the Institute of Physics and Engineering in Medicine (IPEM) in the UK, have extensive recommendations for the quality assurance of radiographic systems [44, 45, 46]. These recommendations focus on the maintenance of the x-ray equipment (e.g. generator, tube) within an acceptable range of operating parameters, and some tests of the detector such as sensitivity, image sharpness, low-contrast detectability, uniformity, dark noise, etc. However, these tests are mainly qualitative and subjective in nature. The DQE is the most widely accepted objective measure of performance and dose efficiency for digital radiographic detector systems [6], and the only metric that describes how close a detector's performance is to scientifically-based ideal. However, DQE measurements are not currently used as a part of any (known) routine quality assurance program. There are two technical reasons for this. The first is that the conventional method to measure the DQE as described in the IEC (International Electrotechnical Commission) 62220-1 [17] standard, is a complex test that requires time, specialized equipment, and a great deal of expertise in analysing

and interpreting the data that's obtained. The second, and most serious reason, is that it is not always easy (or even possible) to obtain linear data from the multitude of imaging system types in clinical use. At the time this thesis was written, a NEMA (National Electrical Manufactures Association) standard is under development that will require manufacturers who subscribe to provide a test mode on their equipment in which proprietary adaptive noise-suppression algorithms can be disabled. This is an important development and recognition of the need to perform proper quality assurance tests. In addition, it is the only condition required for the method of DQE testing developed in this thesis. As a result, the new method described here can be widely adopted for use in clinical environments.

1.6 Research Problems and Objectives

Whether it is result of image processing, or other mechanisms, non-linear image data is a fact of life in the clinical environment. This is the primary impedance to the adoption of DQE measurements in the clinical environment for quality assurance purposes.

Measuring the DQE on clinical systems necessitates an approach that is robust enough to handle the numerous transformations that manufacturers apply. The approaches noted above are important steps towards this objective. However the work described above has also highlighted the important limitations of these approaches. Any method to measure DQE that is useable on the broadest spectrum of x-ray imaging detectors must be applicable in the presence of edge-enhancement, and adaptive non-linear algorithms. After careful consideration of the problem, it is believed that such a method must have the following characteristics:

1. linearization of image data without any foreknowledge of the system characteristic response;

2. derived from images of stationary test objects only, required to ensure that adaptive algorithms or exposure controls do not vary exposure parameters from one image to the next; and

3. derived from images containing only low-contrast test phantoms.

The first characteristic is necessary because the response is usually proprietary and not known at the time of measurement. The reason for the second characteristic is slightly less obvious, but it is because with constant exposure conditions and unchanging images, adaptive algorithms will not be "provoked" in to changing the system response inter-image. The use of only low-contrast attenuators insures that if the form of the response is such that exposures below a certain threshold are truncated to zero (e.g log), the measurements will not be affected.

The objective of this thesis is to develop a experimental technique that implements these characteristic and is therefore able to measure DQE on the broadest range of detectors possible. This will permit DQE measurements to made in a clinical environment where linear data is not provided and allow the DQE to be used in quality assurance programs for the reasons described in the previous section. If the method is successful at accurately measuring the DQE from image data that has been processed it will provide further validation of the DQE as a robust measure of system performance, and an ideal candidate for use in regular quality assurance.

Chapter 2 of this thesis describes the details the method which uses a novel theoretical approach for the linearization of the system response. Some speculation about the possible implications of this are considered in the next section.

1.7 Implications for Clinical Quality Assurance

The development of a method to measure DQE of any system will enable the adoption of DQE measurements in to the quality assurance regime which will have numerous

benefits. One specific benefit will be the greater general awareness among clinical health providers of the DQE, and its importance as a metric that objectively quantifies the dose efficiency of digital radiography systems. This will help providers understand the difference between high- and low-performance systems in terms of impacts on patient dose.

Increased awareness will insure DQE has a greater bearing on purchase decisions which will compel manufacturers to make sure the DQE is as good as it can be in order to be competitive. Improvements in the DQE will improve overall dose efficiency of systems and thereby allow for reduced patient doses. As a specific example of the potential benefits, consider that globally there are approximately 138 million x-ray (radiographic) procedures done annually [1]. If an average dose of 0.25 mSv per procedure is assumed, and this can be reduced by a modest 10% through more discriminating purchase decisions based on DQE specifications, and QA programs that target low-DQE systems for servicing, the population dose can be reduced by approximately 3,450 Sv per year. The average lifetime risk of fatal cancer is somewhere between 3% and 5% per Sievert [10], which implies that approximately 200 premature deaths caused by x-ray procedures could be prevented world wide!

In addition to improved patient safety, routine testing of DQE will enable evidence-based service maintenance and end of life decisions for x-ray detector equipment. The decision to replace a detector could be based on measurements of the DQE, rather then on pressures from vendors about image quality and life expectancy. This could result in tremendous savings if equipment life could be extended by demonstrating, through DQE testing, that system performance is still adequate.

Bibliography

[1] *Medical Imaging Markets*. TriMark Publications, LLC, 2011.

[2] D. J. Brenner, R. D., D. Goodhead, E. Hall, C. Land, J. Lee, J. H. Lubin, D. L. Preston, R. J. Preston, J. S. Puskin, E. Ron, R. K. Sachs, J. M. Samet, R. B. Setlow, and M. Zaider. Cancer risks attributable to low doses of ionizing radiation: Assessing what we really know. *Proceedings of the National Academy of Sciences of the United States of America*, 100:13761–13766, 2003.

[3] ICRP. Icrp publication 103: The recommendations of the icrp. Technical report, (Internationational Commission on Radiological Protection, 2008), 2007.

[4] A. Rose. Television pickup tubes and the problem of vision. In Marston, editor, *Advances in Electronics and Electron Physics*, pages 131–166. Academic Press, 1948.

[5] A. Rose. The sensitivity performance of the human eye on an absolute scale. *Journal of the Optical Society of America*, 38(2):196–208, 1948.

[6] C. E. Metz, R. F. Wagner, K. Doi, D. G. Brown, R. M. Nishikawa, and K. J. Myers. Toward consensus on quantitative assessment of medical imaging systems. [review]. *Med Phys*, 22:1057–1061, 1995.

[7] Boone J. M. *Handbook of Medical Imaging, Volume 1. Physics and Psychophysics*, chapter 1. X-ray production, interaction, and detection in diagnostic imaging, pages 3–77. SPIE Press, 2000.

[8] National Research Council Committee to Assess Health Risks from Exposure to Low Levels of Ionizing Radiation. Health risks from exposure to low levels of ionizing radiation: Beir vii - phase 2. Technical report, National Research Council, 2006.

[9] M.M. Rehani, G. Bongartz, S.J. Golding, L.Gordon, W. Kalender, T. Murakami, P. Shrimpton, R. Albrecht, and K. Wei. Icrp report 87: Managing patient dose in computed tomography. Technical report, Internation Commission on Radiological Protection, 2000.

[10] M. Carter. Variation in the fatal cancer probability per unit effective dose with age at exposure and population statistics. *Radiation Protection Dosimetry*, 60:167–170, 1995.

[11] A. R. Cowen, A. G. Davies, and S. M. Kengyelics. Advances in computed radiography systems and their physical imaging characteristics. *Clinical Radiology*, 62:1132–41, 2007.

[12] J. A. Rowlands. The physics of computed radiography. *Phys Med Biol*, 47(23):R123–R166, Dec 2002.

[13] D. A. Tucker and P. S. Rezentes. The relationship between pixel value and beam quality in photostimulable phosphor imaging. *Medical Physics*, 24:887–893, 1997.

[14] A. Seibert. Tradeoffs between image quality and dose. *Pediatr Radiol*, 34:183–195, 2004.

[15] R. M. Nishikawa and M. J. Yaffe. Signal-to-noise properties of mammographic film-screen systems. *Med Phys*, 12:32–39, 1985.

[16] R. K. Swank. Absorption and noise in x-ray phosphors. *J Appl Phys*, 44(9):4199–4203, 1973.

[17] Characteristics of digital x-ray imaging devices - Part 1: Determination of the detective quantum efficiency. Medical Electrical Equipment IEC 62220-1, International Electrotechnical Commission, 2003.

[18] C. Hwy, L. Seungman, Y. J. Chul, H.K. Kim, M.G.Farrier, T. G. Achterkirchen, M. McDonald, and Cunningham I.A. Characterization of imaging performance of a large-area cmos active-pixel detector for low-energy x-ray imaging. *Nuclear Instruments and Methods in Physics Research*, 652:500–503, 2011.

[19] W. Zhao, G. Ristic, and J. A. Rowland. X-ray imaging performance of structured cesium iodide scintillators. *Med Phys*, 31(9):2594–2605, Sep 2004.

[20] R. Shaw. The equivalent quantum efficiency of the photographic process. *J Photogr Sc*, 11:199–204, 1963.

[21] M. Rabbani and R. L. Van Metter. Analysis of signal and noise propagation for several imaging mechanisms. *J Opt Soc Am A*, 6:1156–1164, 1989.

[22] I. A. Cunningham. Image quality and dose. In J. A. Seibert, L. J. Filipow, and K. Andriole, editors, *Practical Digital Imaging and PACS*, book chapter 8. Advanced Medical Publishing for American Association of Physicists in Medicine, 1999.

[23] "medical imaging - the assessment of image quality". Technical Report 54, ICRU Report 54 (International Commission of Radiation Units and Measurements, Bethesda, MD, 1995).

[24] R. N. Bracewell. *The Fourier Transform and its Applications*. McGraw-Hill, New York, 2 edition, 2000.

[25] J.D. Gaskill. *Linear Systems, Fourier Transforms, and Optics*. Wiley, New York, 1978.

[26] K. Rossmann. Point spread-function, line spread-function, and modulation transfer function. *Radiol*, 93:257–272, 1969.

[27] N. Wiener. Generalized harmonic analysis. *Acta Mathematica*, 55:117–258, 1930.

[28] J. C. Dainty and R. Shaw. *Image Science*. Academic Press, New York, 1974.

[29] I. A Cunningham. *Handbook of Medical Imaging, Volume 1. Physics and Psychophysics*, chapter 2. Applied Linear-Systems Theory, pages 79–156. SPIE Press, 2000.

[30] I. A. Cunningham. Applied linear-systems theory. In J. Beutel, H. L. Kundel, and R. Van Metter, editors, *Handbook of Medical Imaging: Vol 1, Physics and Psychophysics*, Ch 2, pages 79–159. SPIE Press, 2000.

[31] E. Samei, M. J. Flynn, and D. A. Reimann. A method for measuring the presampled mtf of digital radiographic systems using an edge test device. *Med Phys*, 25(1):102–113, Jan 1998.

[32] J. A. Rowlands and D. M. Hunter. X-ray imaging using amorphous selenium: photoinduced discharge (pid) readout for digital general radiography. *Med Phys*, 22(12):1983–1996, Dec 1995.

[33] L. R. Morin and A. Seibert. The standardized exposure index for digital radiography: an opportunity for optimization of radiation dose to the pediatric population. *Pediatr Radiol*, 41:573–581, 2010.

[34] H.S. Park, J.H.J. Kim, C. Lee, and Y.N. Coi. Effects of image processing on the detective quantum efficiency. *Journal of Korean physics society*, 56:653–658, 2010.

[35] M. Analoui. Radiographic digital image enhancement. part ii: transform domain techniques. *Dentomaxillofacial Radiology*, 30:65–77, 2001.

[36] M. Analoui. Radiographic image enhancement. part i: spatial domain techniques. *Dentomaxillofacial Radiology*, 30:1–9, 2001.

[37] M. Prokop and C.M. Shaefer-Prokop. Digital image processing. *European Radiology*, Suppl. 3:73–82, 1997.

[38] W. Hillen, U. Schiebel, and T. Zaengel. Imaging performance of a digital storage phosphor system. *Med Phys*, 14:744–751, 1987.

[39] J. T. Dobbins, D. L. Ergun, L. Rutz, D. A. Hinshaw, H. Blume, and D. C. Clark. Dqe(f) of four generations of computed radiography acquisition devices. *Med Phys*, 22:1581–1593, 1995.

[40] E. Samei and M. J. Flynn. An experimental comparison of detector performance for computed radiography systems. *Med Phys*, 29(4):447–459, Apr 2002.

[41] R. F. Wagner and E. P. Muntz. Detective quantum efficiency (dqe) analysis of electrostatic imaging and screen-film imaging in mammography. In J. E. Gray, editor, *Proc SPIE*, volume 173, pages 162–165, 1979.

[42] P. C. Bunch, K. E. Huff, R. Shaw, and R. L. Van Metter. Comparison of theory and experiment for the dqe of a radiographic screen-film system. In R. H. Schneider and S. J. Dwyer, editors, *Proc SPIE*, volume 535, pages 166–185, 1985.

[43] K. Stierstorfer and M. Spahn. Self-normalizing method to measure the detective quantum efficiency of a wide range of x-ray detectors. *Med. Phys.*, 26:1312–1319, 1999.

[44] "recommended standards for routine performance testing of diagnostic x-ray imaging systems". IPEM Report 91, Insititute of Physcists and Engineers in Medicine, 2005.

[45] J. Shepard and Pei-Jan Paul Lin. Quality control in diagnostic radiology. AAPM Report No. 74, American Association of Physicists in Medicine Task Group 12, 2002.

[46] M. Sieband. Aapm report 4: Basic quality control in diagnostic radiology. Technical report, American Association of Physicists in Medicine, 1977.

Chapter 2

A method to measure the DQE in a clinical setting

This chapter consists of a manuscript ready to be submitted for publication, authored by M. McDonald, H.K. Kim and I.A. Cunningham.

2.1 Introduction

The potential biological risks associated with exposure to ionizing radiation makes it critical that diagnostic x ray imaging systems be designed and maintained to produce the best possible images for a given x-ray exposure. To achieve this, regulatory programs often establish acceptable levels of radiation exposure for common procedures and image-quality tests are designed to evaluate selected performance-based tasks. While scientific and professional communities have made these tests more quantitative than in the pre-digital era, [1, 2, 3, 4] it is widely recognized that x ray systems produce the best possible image quality in terms of image signal-to-noise ratio (SNR) *only* when the detective quantum efficiency (DQE) [5, 6] is as close to unity as possible at all spatial frequencies of importance.

The DQE describes the *equivalent* quantum efficiency [5] of an x ray detector and

is a surrogate measure of the detector "dose efficiency". [7, 8] In addition, since the DQE is proportional to the noise-equivalent quanta (NEQ) which has fundamental importance for the description of radiographic imaging systems as it describes the performance of an ideal observer under certain noise-limited conditions, [9, 10, 11] it is therefore possibly the best indicator of system performance we have.

An expression for the DQE is given by: [5, 7]

$$\mathrm{DQE}(u) = \frac{XQ_oG^2\left|\mathrm{T}(u)\right|^2}{\mathrm{W}(u)} = \frac{\bar{d}^2\left|\mathrm{T}(u)\right|^2}{XQ_o\mathrm{W}(u)} \tag{2.1}$$

where X [mR] is the exposure incident on the detector and projected into the image plane, Q_o [quanta/mm^2/mR] is the number of x ray quanta in the beam per unit exposure, G is the system gain relating $\bar{q}$, the average number of incident quanta per unit area where $\bar{q} = XQ_o$, to $\bar{d}$, the corresponding average dark-subtracted pixel value, and $\mathrm{W}(u)$ is the associated image Wiener noise power spectrum (NPS). This expression is valid for linear and shift-invariant imaging systems, and was adopted by the International Electotechnical Commission (IEC) in a standard method for DQE testing with the substitution $XQ_o = \bar{q} = \mathrm{W}_{\bar{q}}(u)$ as the Wiener NPS of the incident Poisson-distributed quanta in IEC 62220-1. [12]

While the DQE is required for regulatory compliance for new products, and the potential benefits from testing and monitoring the DQE seem obvious for ensuring and documenting optimal system performance, it is part of clinical quality assurance programs in only a small number of leading-edge facilities. [13, 14, 15] There are several reasons for this. For example, DQE measurements generally require an environment where x ray exposure conditions can be controlled and monitored, and clinical instruments cannot always be removed from use for the time it takes to perform DQE testing. An additional impediment for many systems is that while an assessment of the DQE requires access to linear (or linearized [16, 17, 18]) image data, manufac-

turers often implement non-linear image-processing to give images a preferred look. In many cases, these algorithms are considered proprietary and not disclosed to the user, making it difficult or impossible to extract the required linear image data. In addition, they may incorporate adaptive noise-reduction algorithms and automatic exposure control features that depend on certain patient features or exposure conditions. This means both G and $\mathrm{T}(u)$ may be functions of unknown parameters and as a result the system response may be adaptive and vary from one exposure to another, and possibly from one region to another in a single image. These confounding conditions make it difficult or impossible in many cases to perform standards-compliant DQE testing.

In this chapter, a method is described for measuring the DQE that can be implemented on both linear and non-linear systems. It differs to a standards-based method (IEC) in two ways: 1) image data is linearized using what is called a "neutral-attenuator" method; and 2) a semi-transparent edge with a modest attenuation (15-20%) is used to determine the small-signal MTF. Since the analysis uses measurements of only low-contrast features in otherwise uniform images, even non-linear or adaptive image-processing is approximately linear (essentially a first-order Taylor expansion of $\mathrm{T}(u)$ in terms of X). This linearized small-signal (LSS) approach is validated by comparing the LSS DQE obtained using both processed (non-linear) and raw (linear) image data with a standards-compliant DQE on the same system.

2.2 Theory

2.2.1 Linearizing System Response: the Neutral-Attenuator Method

For an ideal linear detector, the average dark-subtracted pixel value $\bar{d}$ is proportional to the average x ray energy deposited in the pixel, E_d [keV]:

$$\bar{d} = kE_d = ka\hat{E}, \tag{2.2}$$

where k [keV^{-1}] is a constant of proportionality, a [mm^2] is the pixel area, $\hat{E}$ [keV mm^{-2}] is the area density of deposited energy given by

$$\hat{E} = \bar{q}E_q = \bar{q}\int_0^{kV} s(E)\alpha(E)E_a(E)\mathrm{d}E, \tag{2.3}$$

$\bar{q}$ [mm^{-2}] describes a uniform Poisson distribution of x ray quanta incident on the detector, E_q [keV] is the average energy deposited per incident x ray photon, $s(E)$ is the normalized x ray spectrum where $\int_0^{kV} s(E)\mathrm{d}E = 1$, $\alpha(E)$ is the detector quantum efficiency, and $E_a(E)$ [keV] is the average x ray energy deposited in the detector by a photon having energy E.

The fundamental measurement of all x ray detectors is directly related to deposited energy E_d where $E_d = a\bar{q}E_q$, and digital post-processing algorithms act on this quantity. It therefore seems reasonable to express the average pixel value of both linear and non-linear systems more generally in the form $\bar{d} = f(E_d)$. A key benefit of this representation is that the function f will normally be well behaved over the useful range of exposures, such as a constant of proportionality or a log transformation. A robust inverse transformation can therefore be defined such that $E_q = \frac{1}{a\bar{q}}f^{-1}(\bar{d}) \equiv f_q^{-1}(\bar{d})$ which can be determined by mapping E_q values as a function

of $\bar{d}$, giving a linearized pixel value $\bar{d}_{\mathrm{L}} = k_{\mathrm{L}} a\bar{q} f_q^{-1}(\bar{d})$ where k_{L} is a new constant of proportionality.

The form of f_q^{-1} could be obtained by attenuating a beam with a specified material if not for beam-hardening effects, although it may be possible to construct an attenuator that would attenuate all energies by the same fraction by combining two or more materials that do not have K-edge energies in the useful energy range. As an alternative, we use a material having linear attenuation coefficient $\mu(E)$ [cm^{-1}] and thickness t [cm] combined with a theoretical correction for beam hardening. With this approach, E_q becomes a function of attenuator thickness t:

$$E_q(t) = \int_0^{kV} s(E)\alpha(E)E_a(E)\mathrm{e}^{-\mu(\mathrm{E})\mathrm{t}}\mathrm{d}E. \tag{2.4}$$

The shape of $f_q^{-1}(\bar{d})$ is then determined by plotting measured pixel values $\bar{d}$ as a function of $E_q(t)$ determined theoretically from Eq. (2.4). This linearization transformation is used to convert the series of images with average pixel value $\bar{d}$ into images with average linearized pixel value $\bar{d}_{\mathrm{L}}$.

2.2.2 Linearized Small-Signal (LSS) MTF

The linearized small-signal MTF is determined using a semi-transparent slanted-edge method [19, 20, 21, 22] with the edge thickness chosen to attenuate the primary beam by 15 - 20%. The small attenuation is necessary to avoid a problem on some systems where low exposure values are truncated to zero, which would cause loss of information about PSF tails.

Use of a semi-transparent edge introduces a complication caused by scatter emitted from the edge that may contribute to the measured profile. Based on the work of Neitzel *et. al* [21], it can be shown that an MTF measured using the semi-transparent edge method, $\mathrm{T_S}(u)$, is related to the true MTF, $\mathrm{T}(u)$, by

$$\mathrm{T_S}(u) \approx \mathrm{T}(u) \left\{ \frac{1}{1+\gamma/\beta} + \frac{1}{1-\beta/\gamma}\mathrm{S}(u) \right\} \tag{2.5}$$

where β is the edge-attenuation factor, γ is the edge-scatter-to-primary ratio in x-ray intensity at the image plane behind the edge, and $\mathrm{S}(u)$ is the Fourier transform of the (normalized) scatter point-spread function. In practise, γ decreases with increasing detector distance and an accurate MTF measurement is obtained by choosing a distance that ensures $\gamma \ll \beta$. Copper was chosen as the edge material as the majority of x-ray interactions are photoelectric and the resulting characteristic emissions have a very low energy ($\sim$9.0 keV), thereby minimizing the effect caused by edge scatter.

2.2.3 Linearized Small-Signal DQE

Using linearized images to determine the linearized small-signal MTF $\mathrm{T_L}(u)$ and NPS $\mathrm{W_L}(u)$, gives the small-signal DQE equation assumes the familiar form:

$$\mathrm{DQE_L}(u) = \frac{\bar{d}_\mathrm{L}^2 |\mathrm{T_L}(u)|^2}{XQ_o\mathrm{W_L}(u)}. \tag{2.6}$$

2.3 Detector Glare

Detector glare results from large area scattering of x rays, electrons and optical photons [23]. This may result in long-range tails in the system PSF and scales with $\bar{q}$ for uniform exposures of the detector. This causes a complication when determining system gain G in Eq. 2.1 using the LSS method due to the fact that the steps cover only a small fraction of the detector making the glare component approximately constant in each step. It is therefore useful to write $\bar{d} = \bar{d}_s + \bar{d}_g$ where $\bar{d}_g$ is the glare component and scales with $\bar{d}_s$ for uniform exposures. Accordingly, it is convenient to separate the system gain into two terms:

$$G = \frac{\overline{d}}{\overline{q}} = \frac{\overline{d}_s}{\overline{q}} + \frac{\overline{d}_g}{\overline{q}} = G_s + G_g.$$

Gain G is the true system gain and could be measured by adjusting the intensity of a uniform exposure, while G_s is the gain determined using the LSS method where the glare term is approximately constant.

In Fig. 2.1a the linearization of a linear system with glare is shown. The true gain of the system G is the ratio of pixel value $\overline{d}$, to measured $\overline{q}$. Theory does not account for glare, ($\overline{d}_g$=0), and thus predicts that the measured pixel value should be $\overline{d}_s$ and the gain should be G_s. The discrepancy means that the response measured in the LSS method will therefore have slope G_s and offset $\overline{d}_g$. As a consequence, noise in linearized images will be increased by the factor $|G_s/G|^2$, and noise measured by the LSS method will be given by:

$$\mathrm{W_L}(u) = \left|\frac{G}{G_s}\right|^2 \mathrm{W}(u).$$

Fig. 2.1b shows the linearization of a hypothetical non-linear system. The system has a gain of G at the point of measurement. The gain of the linearized system response is $1/G_s$, where again G_s is the gain of the system at the point of measurement in the absence of glare.

2.4 Methods

The linearized small-signal DQE method was implemented using images from a General Electric Revolution QX/i digital radiography flat panel detector. This system provides both "processed" and "raw" images for each exposure. The processed images have an inverted gray scale and some edge enhancement that is based on user settings with an unknown algorithm and cannot be completely disabled. The raw images have a linear response and no edge enhancement. These differences are illustrated

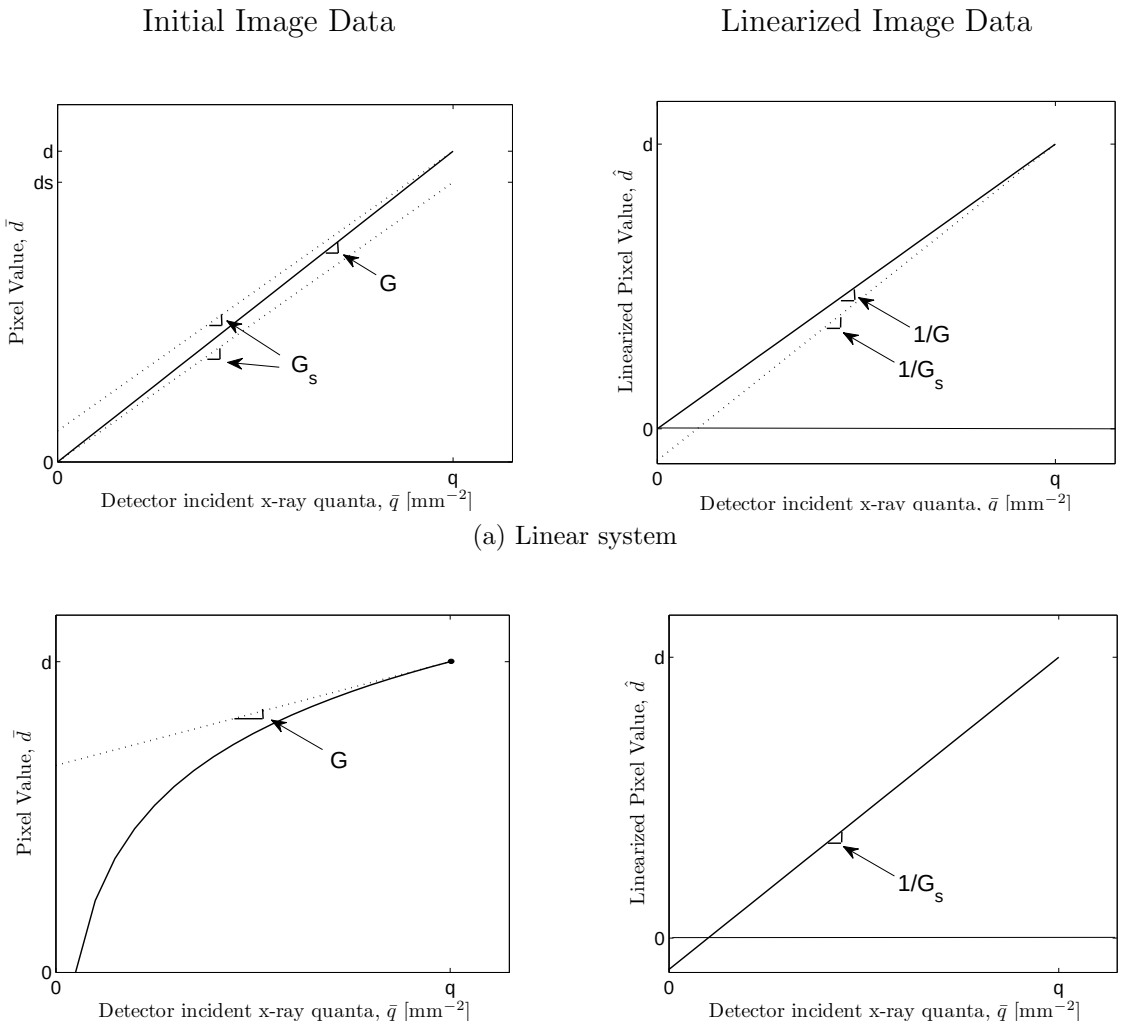

(a) Linear system

(b) Non-linear system

Figure 2.1: Linearization of the system from initial response, to linearized response for (a) a linear system with glare and (b) a hypothetical non-linear system.

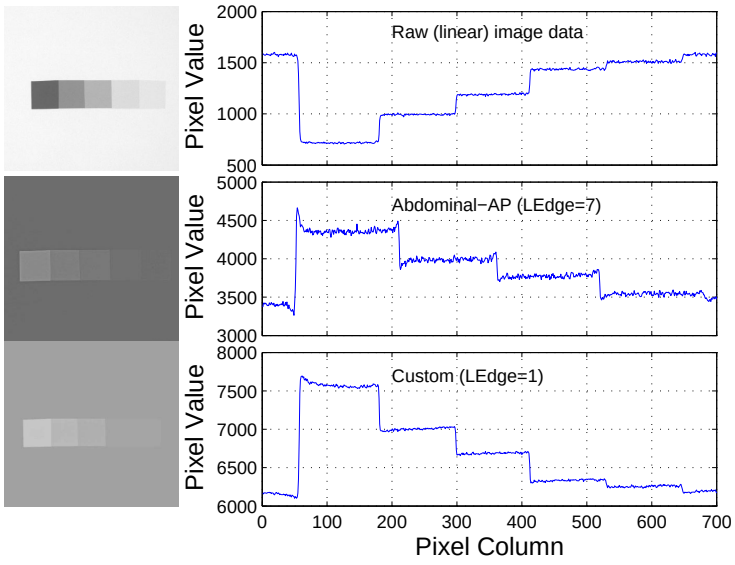

Figure 2.2: Images of a copper step wedge and corresponding profiles of pixel values. Three different protocols are shown: raw (linear), abdominal-AP (LEdge=7), and the custom setting used in these experiments (LEdge=1) .

in Fig. 2.2 which shows profiles through images of a copper step-wedge attenuator. The small-signal MTF and DQE were determined using both raw and processed images, and validated by comparing with separate MTF and DQE measurements made following the IEC standard[12] using raw images.

2.4.1 Linearizing System Gain

The linearization transformation f_q^{-1} was determined using measured pixel values $\bar{d}$ and theoretical $E_q(t)$ values from Eq. (2.4) for known thicknesses t of copper shim stock (forming a stepwedge with nominal thicknesses 0.025, 0.051, 0.152, 0.254 and 0.457 mm and with a nominal accuracy of 10% stated by the supplier[24]) for an RQA-5 spectrum (70 kV, 21 mm added Al and a verified HVL of 7.1 mm Al). Copper linear attenuation coefficients μ were obtained from the NIST database [25] using a copper density of 8.96 g/cm^3.

The pixel value measured using the copper shim can be inflated by scatter generated in the attenuator. A simple model of the measured pixel value is given by:

$$\overline{d} = \overline{d}_p + \overline{d}_e.$$

Where $\overline{d}_p$ is the contribution to pixel value of the primary transmitted x-ray beam, and $\overline{d}_e$ is the contribution from scatter. The value of $\overline{d}$ approaches the value of $\overline{d}_p$ as $\overline{d}_e$ approaches zero which occurs as the distance of the attenuator from the detector is increased. The error in the measured pixel value is given by:

$$\frac{\overline{d} - \overline{d}_p}{\overline{d}_p} = \frac{\overline{d}_e}{\overline{d}_p} = \gamma.$$

The value of γ can be measured as function of distance by gradually increasing the distance of an attenuator from the detector and measuring the attenuated pixel value. The attenuated pixel value is $\overline{d}$, and $\overline{d}_p$ is the value of $\overline{d}$ which is no longer changing with distance. The value of γ was measured for a .018" (.457 mm) thick copper shim and is shown in Fig. 2.3. This is the thickest copper step and will provide a worst case scenario of the scatter-to-primary ratio. For the measurement of f_q^{-1} , the copper was placed at a distance of 200 mm from the detector cover where the error in pixel value due to scatter is less then 0.5%.

The detector quantum efficiency α was estimated as the probability of interaction assuming 0.471 g/cm^2 of CsI and a 1 mm thickness. The form of f_q^{-1} was determined from a second-order polynomial fit of $\bar{d}$ as a function of $\hat{E}_q$. The accuracy of this method is dependent on having an x-ray spectrum with a half-value layer (HVL) that accurately conforms to the RQA-5 standard, and copper steps of known thickness. The HVL was measured and confirmed to be within 1% of the nominal 7.10-mm Al value. Copper thicknesses were measured with a micrometer and verified to agree with nominal values ±0.003 mm (the accuracy of the measurement). A discussion on the accuracy of the method is included in the results section. The neutral-attenuator method was validated by verifying that f_q^{-1} is a linear transformation when deter-

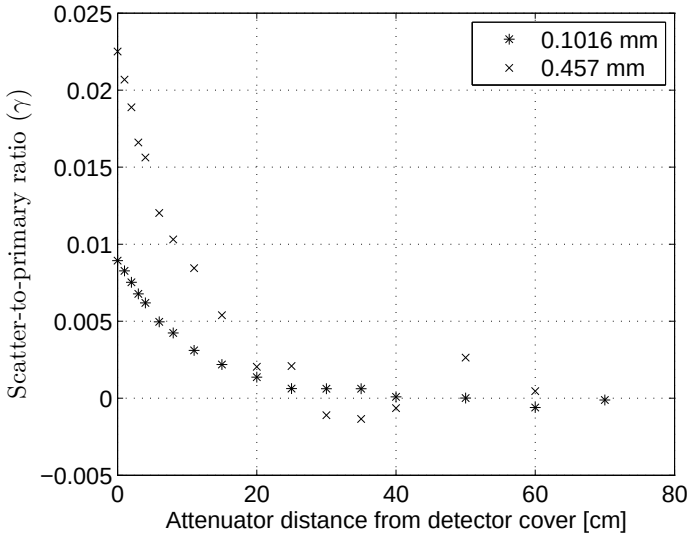

Figure 2.3: Scatter-to-primary ratio for copper shim as a function of attenuator distance from detector cover for the thicknesses shown.

mined using raw image data.

2.4.2 Small-Signal MTF

The small-signal MTF edge was created from 0.004" (0.102 mm) copper with a carefully machined edge. While use of thin copper shim makes the method less sensitive to rounded corners on the edge profile than a thick edge, a rounded profile could still reduce the MTF at high spatial frequencies. A worst case estimate of the error in $\mathrm{T_L}(u)$ due to scatter from the copper edge was made using Eq. (2.5) with the assumption that $S(u > 0) = 0$. The scatter-to-primary fraction γ for the copper edge was measured as function of edge-detector distance, and the data is plotted in Fig. 2.3. The results for selected distances are shown in Table 2.1. For a distance of 200 mm, the value of γ was determined to be approximately .1%, thereby resulting in less then 1% inflation of the MTF. This provides an upper bound on the distance that it's necessary to measure the MTF to eliminate scatter. To determine the optimal distance, the measurement was made with at 0, 50, 100, and 200 mm. For each distance the accuracy of the small-signal MTF was validated by comparison with an

Edge-detector distance [mm]	γ	β	$\frac{1}{1+\gamma/\beta}+\frac{1}{1-\beta/\gamma}\mathrm{S}(u)$
0	.009	.21	1.05
50	.006	.21	1.03
100	.003	.21	1.01
200	.001	.21	1.005

Table 2.1: The error in MTF due to scatter is calculated as a function of edge-detector distance for a .004" (0.1016 mm) copper edge. This is a worst case scenario, where the assumption is that $S(u > 0) = 0$. For the error in MTF due to scatter to be less then 1% the edge must be placed >200 mm from the detector cover.

IEC MTF [12] using a 3-mm tungsten edge and raw (linear) dark-subtracted, but not linearized image data. A 100-mm region of interest (ROI) spanning across the edge by 25 mm along the edge was used to determine the MTF.

2.4.3 Linearized Small-Signal MTF

The linearized small-signal (LSS) MTF is similar to the small-signal MTF but uses linearized image data. Validation of the LSS MTF was obtained by comparing the MTF obtained using raw-image data with linearized image data.

2.4.4 NPS and DQE

The frequency-dependent NPS was calculated using an open-field area in four images. The IEC value of Q_o for the RQA-5 spectrum was used. The linearized small-signal DQE obtained using Eq. (2.6) with both raw (linear) and processed (non-linear) image data was compared with an IEC 62220-1 [12] compliant DQE obtained using the 3-mm tungsten edge and a four open-field images for the calculation of the NPS.

2.5 Results

2.5.1 System Gain

A comparison of theoretical $\hat{E}_q$ values from Eq. (2.4) with measured pixel values $\bar{d}$ from raw images is shown as a function of copper thickness in Fig. 2.4. For this test, the copper was placed in two configurations: one in which the stepwedge is centered in the image, and one in which it is placed at the image edge. While there is reasonably good agreement with the theoretical deposited energy in both cases, pixel values become slightly inflated with increasing copper thickness. It was found that this phenomenon is caused by veiling glare, confirmed by placing the copper in a "narrow beam" geometry wherein the x-ray beam was tightly collimated to the copper pieces. In this configuration the discrepancy between measured pixel values and theoretical deposited energy was greatly reduced [26]. For the "centered" configuration, there is an approximately 5% additive term from glare which is consistent with the 5% low-frequency drop observed in the IEC-compliant MTF. For the "edge" measurement, the additive term is of the order 2-3% where reduced glare is expected. It is important to note that the small disagreement in Fig. 2.4 is not an error. Rather, it shows that for linear image data, pixel values are proportional to theoretical $\hat{E}_q$ values plus a component due to glare in the detector. For the measurement f_q^{-1} , the copper steps were placed in the "edge" configuration in order to take advantage of the reduced glare.

The transformation to linearized pixel value, f_q^{-1} is shown in Fig. 2.5 for both raw and processed images. As expected, the transformation is a straight line for the raw image data. The fact that it does not pass through the origin is due to the 2-3% glare offset. (It is interesting to note, therefore, that by using f_q^{-1} to linearize image data, the linearized image is approximately corrected for detector glare. This observation is true only for images containing very little image contrast, such as is used in this

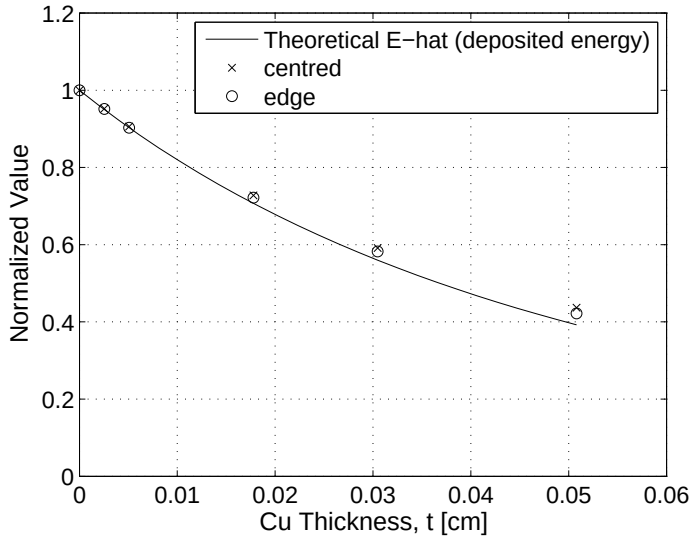

Figure 2.4: Comparison of normalized theoretical $\hat{E}_q(t)$ values with normalized $\bar{d}$ values determined from linear image data as a function of copper thickness t. The "centered" data is the configuration in which copper is centered in the image, while "edge" refers to the configuration in which copper is placed at the image edge. In each case, the small difference in increasing thickness is due to a offset in pixel value caused by detector glare.

study, where detector glare is approximately uniform across the image). The result of this is an increase in the system gain by 2-3% which may introduce an error by this amount in the DQE. The processed image data shows an inverted gray scale. In both cases, the transformation is well behaved as expected.

2.5.2 Small-Signal MTF

In Fig. 2.6a the small-signal MTF using linear dark-subtracted, flat-field corrected data is shown for the four edge-to-detector-cover distances tested. The MTF using the IEC compatible opaque edge is shown in Fig. 2.6b for the same distances. In both figures an effect of declining MTF with distance can be observed. The 0 mm and 50 mm measurements are indistinguishable, however the measurement at 100 mm and 200 mm are in error by 5% and 18% respectively at 2.5 mm^{-1}. This effect may be

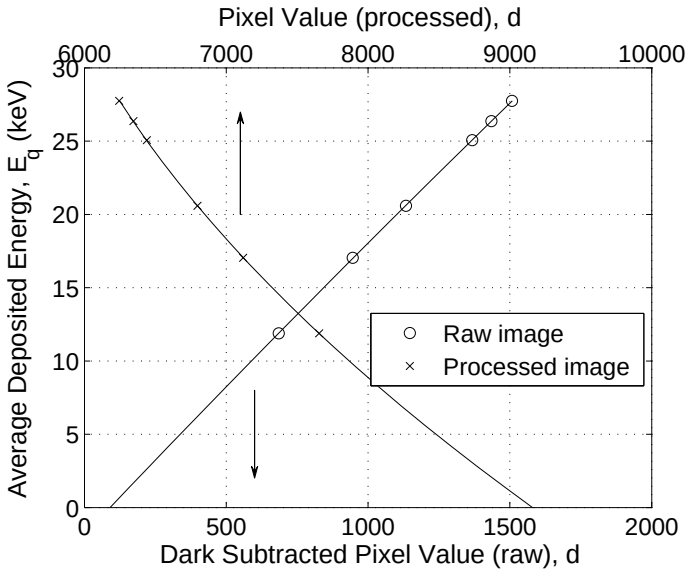

Figure 2.5: The form of f_q^{-1} is given by this plot of deposited energy $\hat{E}_q$ (proportional to linearized pixel value) vs. measured pixel value $\bar{d}$. For processed image data, it can be trusted only between the first and last data point.

due to a penumbral blur resulting from off-axis x rays created by the finite focal-spot, and scatter from beam hardening filtration. Fig. 2.7 compares the small-signal MTF using linear image data with an IEC MTF for each distance tested. Excellent agreement is seen for the 100 mm and 200 mm data. Good agreement is seen in the 1 mm and 50 mm data except at low frequencies where, as was anticipated, there is a small but non-trivial increase in the small-signal MTF. A distance of 50 mm was selected to be used for the measurement of DQE. An explanation of this choice is left to the discussion section.

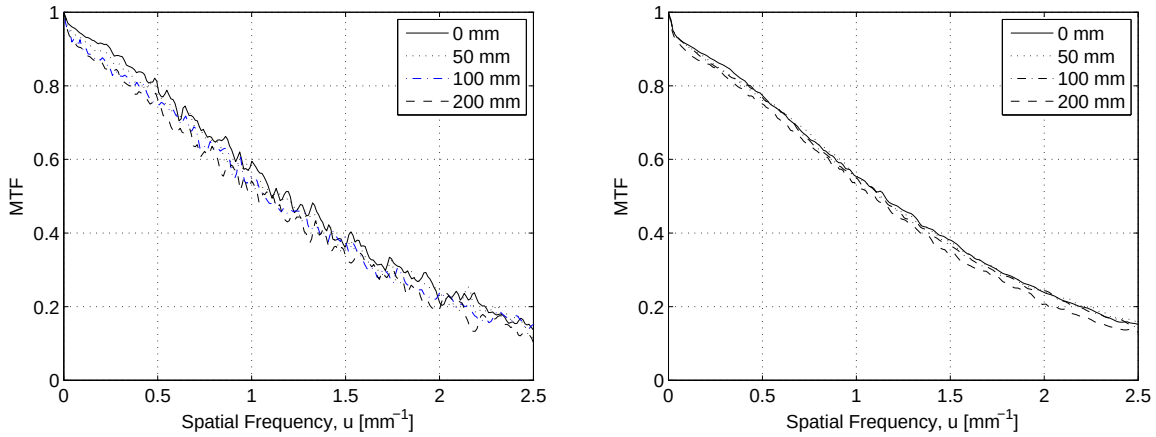

(a) Small-signal MTF (b) IEC MTF

Figure 2.6: Comparison of the small-signal MTF measured using the semi-transparent edge with a conventional IEC method when the edge is placed 0, 50, 100 and 200 mm from the detector cover, using linear image data.

2.5.3 Linearized Small-Signal MTF

Figure 2.8 shows a comparison of the linearized small-signal MTF, obtained using both raw and processed image data, with an IEC-compliant MTF with the exception that a 15 mm window was used rather than 100 mm in the MTF measurement. This was to reduce the effects of x-ray beam inhomogeneity in the calculation of MTF from (linearized) processed data, where no flat-field corrections could be performed. Using a small window truncates the LSF tails, and thereby decreases the low-frequency drop. With this change, the small-signal and IEC results are equivalent. However, since there is no low-frequency drop, this means the LSS MTF is scaled up by the amount of the low-frequency drop which is equal to the glare fraction when it is normalized to unity at zero frequency.

Each curve in Fig. 2.8 is an average based on five realizations of the measurement. The small-signal MTF obtained with processed image data shows evidence of edge enhancement.

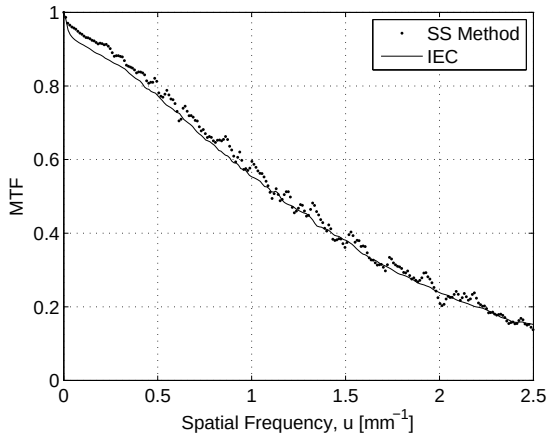

(a) 0 mm

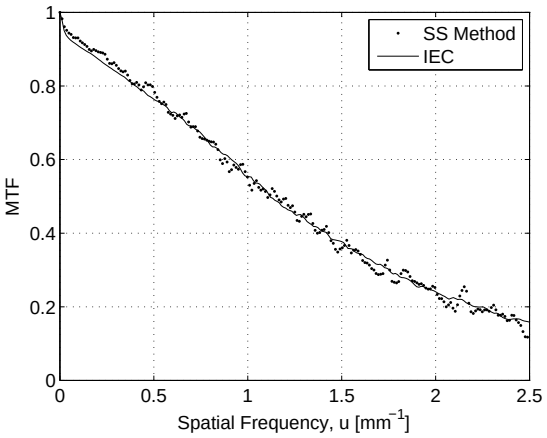

(b) 50 mm

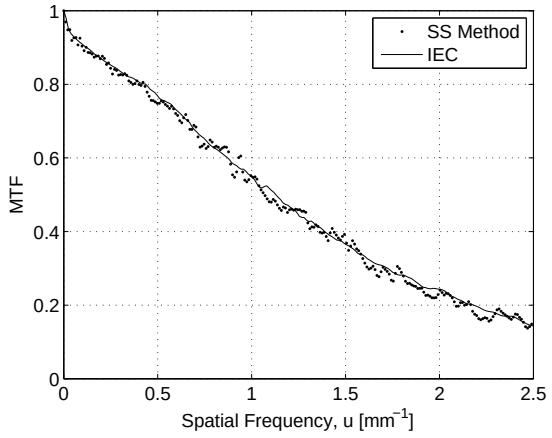

(c) 100 mm

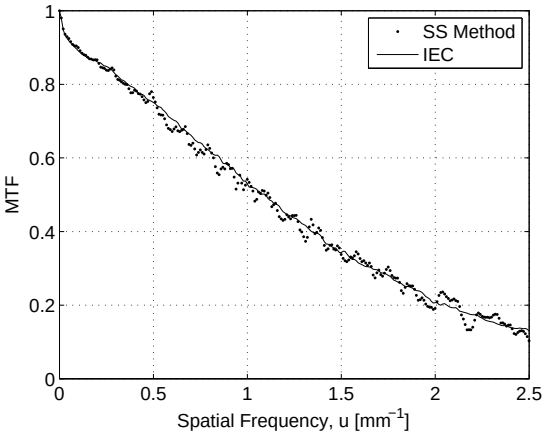

(d) 200 mm

Figure 2.7: Comparison of the small-signal MTF with an IEC MTF with the edge placed 0, 50, 100 and 200 mm from the detector cover, using linear image data.

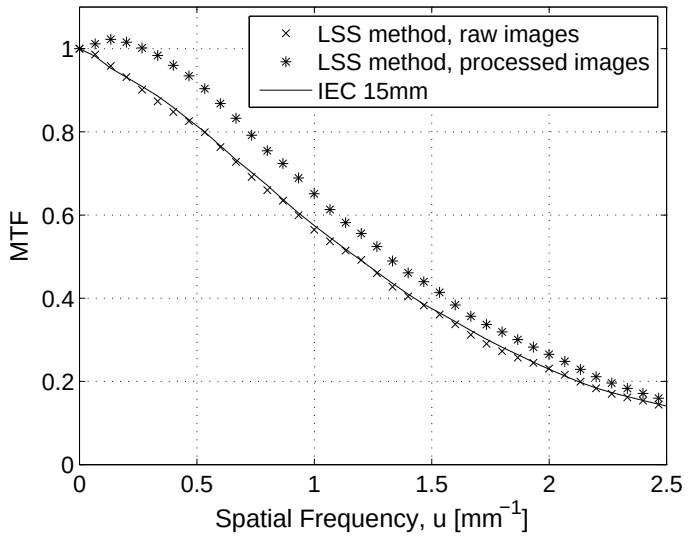

Figure 2.8: Comparison of the LSS-MTF measured from both raw and processed image data with a conventional (IEC) MTF obtained using raw image data. The LSS-MTF does not show the low-frequency drop but does show the effect of edge enhancement in the processed images. All curves are an average of five realizations of the respective measurements.

2.5.4 NPS and DQE

Figure 2.9 shows a comparison of the Wiener NPS (normalized by squared pixel value) obtained using the linearized small-signal approach, using both raw and processed image data, with an IEC NPS. Each curve is the result of averaging five realizations of the measurement. The uncertainty bars represent the standard error for each frequency of the LSS raw and IEC measurements. The error bars overlap for the majority of frequencies however the measurement from raw data has undergone linearization with f_q^{-1}, and appears to be a few percent greater then the IEC measurement which is consistent with the increase in system gain of 2-3%. The NPS from processed data is substantially greater which indicates that image-processing has increased noise. Fig. 2.10 compares the results of the IEC DQE measurement with the LSS method, (both are based on five realizations of the measurement). In this test, the semi-transparent edge was 50 mm from the detector cover. The IEC method requires the opaque edge to be as close to the image plane as physically pos-

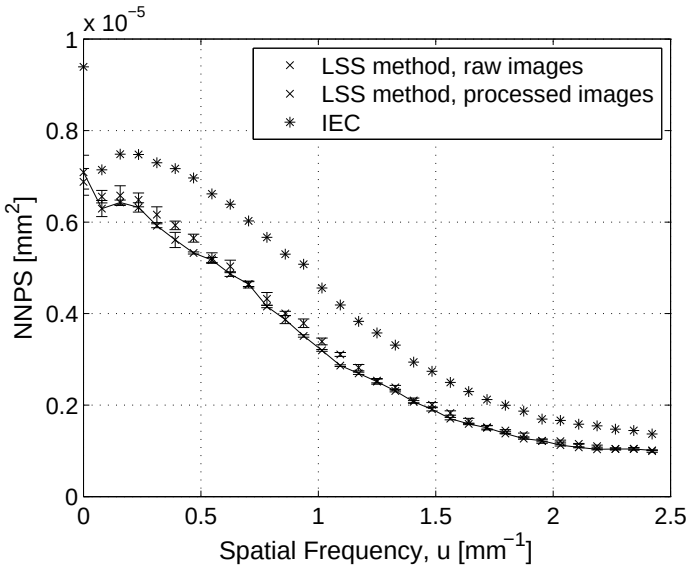

Figure 2.9: Wiener NPS, normalized by squared pixel value, as determined from raw and processed images. All curves are an average of five realizations of the respective measurements.

sible, and therefore a distance of 0 mm was used from the edge to detector cover. All MTF calculations used a 15 mm window. In this configuration, the raw and processed LSS measurements agree well with one another, however they underestimate the IEC measurement by a few percent. The LSS raw measurement is on average 5% less then the IEC measurement. The uncertainty bars represent the standard error for each frequency of the LSS raw measurement. For clarity in the figure, no other error bars are shown, however the uncertainty in the IEC measurement overlaps that of the LSS raw measurement for the majority of frequencies.

2.5.5 Error Analysis

Accuracy of the DQE results will depend on how accurately the parameters required for Eq. (2.4) are known. These include the spectral shape s, quantum efficiency α which depends on detector material and thickness, and mass loading ρt of copper. The relative change in DQE values resulting from a change in each parameter,

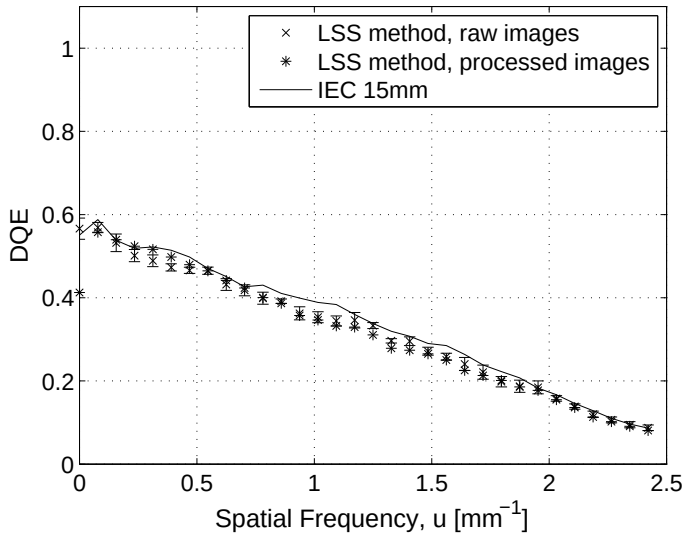

Figure 2.10: DQE determined from raw and processed images. The conventional IEC measurement from linear image data is shown for comparison. All curves are an average of five realizations of the respective measurements. Uncertainty bars for the LSS measurement represent the standard error of the measurement.

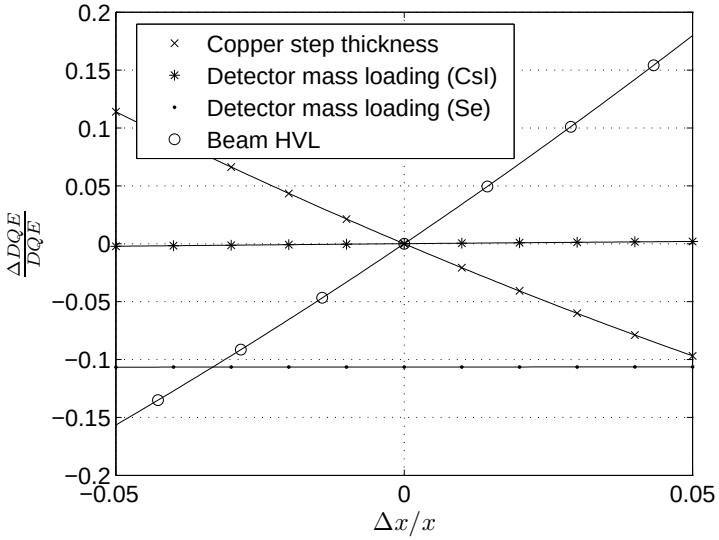

Figure 2.11: Analysis of error in DQE value due to uncertainty in parameter x, where x is Copper step thickness, x-ray beam hvl, and detector mass loading for Se and CsI based detectors.

Parameter (x)	$\frac{\Delta DQE/DQE}{\Delta x/x}$	Required Accuracy
x-ray beam HVL	3.4	0.6%
Copper step thicknesses	-2.1	1%
Detector mass loading (Se)	0.0022	900%
Detector mass loading (CsI)	0.041	48%

Table 2.2: Fractional change in DQE values relative to a change in each parameter x. The third column shows the required accuracy of each parameter to ensure a maximum 2% effect on the DQE.

$^{\Delta DQE/DQE}/_{\Delta x/x}$ with x representing the parameter, was determined by varying each parameter in Eq. (2.4) as illustrated in Fig. 2.11 and Table 2.2.

The IEC standard claims that the DQE can be measured to an accuracy of 5%. To achieve this accuracy using the linearized neutral attenuator approach, it is required that the error from any one parameter must not exceed 2%. It is shown that to achieve this, the HVL must agree with the standard value within 0.6%, and the thickness of copper steps must be accurate to approximately 1% of the larger step thickness. It was also shown that 50% change in detector material thickness resulted in less than a 2% change in DQE. However, incorrectly assuming a Se detector when actually using a CsI detector caused a 10% error.

2.6 Discussion

2.6.1 System Gain

The neutral-attenuator method converts raw and processed to proportional linear deposited energy. If glare is present, it increases the system gain in the linearized response by the glare fraction. On this system there is a glare component of approximately 5% over the majority of the image except very near the image edge where it reduces to 2-3%. For the measurement of system response, the copper was near

the image edge thus resulting in an increase of system gain by 2-3% in the linearized response.

2.6.2 MTF

The use of a semi-transparent edge to measure MTF introduces the problem of scatter from the edge. This is seen as the inflation at low-frequencies in the small-signal MTF. To minimize the effect of scatter, it was found that the measurement must be made with the edge> 100 mm from the detector cover. However, there is a simultaneous problem of the observed drop in the MTF as distance increases, possibly due to off-axis x-rays and the resulting penumbral blur. For a 200 mm edge-detector distance and using an IEC edge this error was approximately 18% @ 2.5 mm^{-1}. If it's assumed that this reduction in MTF applies equally to the small-signal measurements, for which there is good evidence in the generally good agreement of IEC (no scatter) and small-signal MTF measurement for each of the edge-detector distances considered, making the small-signal measurement at 200 mm would create an unacceptable level of error. Some scatter must therefore be tolerated and the measurement of small-signal MTF made at a more moderate distance. In this case the measurement was made at 50 mm. This greatly reduces (but does not eliminate) scatter and the resulting inflation of MTF at low-frequencies, however the greater detector distance with respect to the IEC measurement (which by definition is made at 0 mm distance), could result in a small reduction in small-signal MTF. This effect is presumed to be present but at a distance of 50 mm, is not perceptible. Additionally the use of the small 15 mm window for the calculation of both small-signal and IEC MTF (with the resulting loss of low-frequency drop), has reduced the effects of scatter.

2.6.3 NPS and DQE

The normalized NPS from linearized raw data appears to be greater then the normalized NPS by a few percent. It was demonstrated in the theory section that glare should result in an increase in the system gain and NPS. The 5% difference observed here is consistent with the increase in system gain of 2-3%, which is squared in the NPS. The increase in normalized NPS is responsible for the small difference that's seen in IEC and LSS method DQE measurements. The difference is about 5% therefore this is the accuracy of the LSS method on this system.

The LSS processed DQE measurement agrees extremely well with the LSS raw DQE measurement which leads to the observation that image-processing does not increase the DQE.

2.6.4 Error Analysis

Some implications of the error analysis on the uncertainty in the DQE results are now considered. The copper step thickness must be known to within 1% to achieve less then 2% error in the DQE, although the stated uncertainty by the manufacturer is 10%, measurement of copper thickness with a micrometer with an accuracy of $\pm$.003 mm where identical to the nominal values within this measurement accuracy. Given this accuracy, the uncertainty in the thickness of the .025 mm (thinnest) step is still 10%, however for the thicker steps which are composed of thicker copper, this uncertainty is improved substantially. This provides confidence that the accuracy is better then the manufacturer suggests, and an accuracy of 1% is therefore not an unreasonable assumption. The x-ray beam HVL is known to be within 1% of the nominal 7.1 mm, this uncertainty is slightly greater then the .6% predicted by the error analysis that's required to keep the error in DQE under 2% however it results only in a small increase to 3.4%. The other source of error, the detector mass loading is only required to be known within approximately 50% for CsI, which provides a wide

margin for error, and the estimate used is almost certainly within this range. The total uncertainty from these contributing factors is approximately 6%. The measurement of DQE from raw data is within 6% of the IEC (true) measurement, therefore within the uncertainty of the measurement these are the same.

2.7 Conclusions

A new method has been developed to measure the DQE of non-linear imaging systems. The method uses the concept of a "neutral attenuator" to map the response of the system as a function of theoretical deposited energy and thus linearize the image data. It is the first method to allow the DQE measurement to be made so that all components of the equation are captured from a single static image, which permits the measurement to be made on any system, linear, non-linear, and those that employ adaptive processing. The method was validated on CsI-based digital flat panel detector using linear and processed image data. The results where within a few percent of the conventional IEC DQE measurement. The small discrepancy was caused by glare and the increased system gain resulting from linearization to theoretical deposited energy. The accuracy is expected to be improved on systems where glare is not as prevalent.

The non-availability of linear data is the primary technical impedance to regular monitoring of the DQE in a clinical setting. The linearized small-signal DQE method described here solves this problem and will allow DQE measurements to be incorporated into routine quality assurance programs for constancy testing, acceptance testing, and end of life decision making.

Bibliography

[1] A. R. Cowen, J. M. Haywood, A. Workman, and O. F. Clarke. A set of x-ray test objects for image quality control in digital subtraction fluorography: I. design considerations. *Br. J. Radiol.*, 60:1001–9, 1987.

[2] C. Walsh, D. Gorman1, P. Byrne, A. Larkin, A. Dowling, and J. F. Malone. Quality assurance of computed and digital radiography systems. *Radiation Protection Dosimetry*, 129:271–275, 2008.

[3] "recommended standards for routine performance testing of diagnostic x-ray imaging systems". IPEM Report 91, Insititute of Physcists and Engineers in Medicine, 2005.

[4] J. Shepard and Pei-Jan Paul Lin. Quality control in diagnostic radiology. AAPM Report No. 74, American Association of Physicists in Medicine Task Group 12, 2002.

[5] R. Shaw. The equivalent quantum efficiency of the photographic process. *J Photogr Sc*, 11:199–204, 1963.

[6] J. C. Dainty and R. Shaw. *Image Science*. Academic Press, New York, 1974.

[7] I. A. Cunningham. Applied linear-systems theory. In J. Beutel, H. L. Kundel, and R. Van Metter, editors, *Handbook of Medical Imaging: Vol 1, Physics and Psychophysics*, Ch 2, pages 79–159. SPIE Press, 2000.

[8] I. A. Cunningham and J. Yao. Cascaded models and the DQE of flat-panel imagers: noise aliasing, secondary quantum noise and reabsorption. volume 4682 of *Proc SPIE*, pages 61–72, 2002.

[9] "medical imaging - the assessment of image quality". Technical Report 54, ICRU Report 54 (International Commission of Radiation Units and Measurements, Bethesda, MD, 1995).

[10] K. J. Myers. Ideal observer models of visual signal detection. In J. Beutel, H. L. Kundel, and R. L. Van Metter, editors, *Handbook of Medical Imaging: Vol 1. Physics and Psychophysics*, Ch 9, pages 559–592. SPIE Press, 2000.

[11] H. H. Barrett and K. Myers. *Image Science: Mathematical and Statistical Foundations*. Wiley, New York, 2004.

[12] Characteristics of digital x-ray imaging devices - Part 1: Determination of the detective quantum efficiency. Medical Electrical Equipment IEC 62220-1, International Electrotechnical Commission, 2003.

[13] K. Stierstorfer and M. Spahn. Self-normalizing method to measure the detective quantum efficiency of a wide range of x-ray detectors. *Med. Phys.*, 26:1312–1319, 1999.

[14] I. A. Cunningham. Use of the detective quantum efficiency in a quality assurance program. In *Proc SPIE*, volume 6913, 2008.

[15] N.W. Marshall, A. MacKenzie, and I.D. Honey. Quality control measurements for digital x-ray detectors. *Phys. Med. Biol*, 56:979–999, 2011.

[16] P. C. Bunch, K. E. Huff, R. Shaw, and R. L. Van Metter. Comparison of theory and experiment for the dqe of a radiographic screen-film system. In R. H. Schneider and S. J. Dwyer, editors, *Proc SPIE*, volume 535, pages 166–185, 1985.

[17] J. T. Dobbins, D. L. Ergun, L. Rutz, D. A. Hinshaw, H. Blume, and D. C. Clark. Dqe(f) of four generations of computed radiography acquisition devices. *Med Phys*, 22:1581–1593, 1995.

[18] E. Samei and M. J. Flynn. An experimental comparison of detector performance for computed radiography systems. *Med Phys*, 29(4):447–459, Apr 2002.

[19] P. F. Judy. The line spread function and modulation transfer function of a computed tomographic scanner. *Med Phys*, 3:233–236, 1976.

[20] E. Samei, M. J. Flynn, and D. A. Reimann. A method for measuring the presampled mtf of digital radiographic systems using an edge test device. *Med Phys*, 25(1):102–113, Jan 1998.

[21] U. Neitzel, E. Buhr, G. Hilgers, and P. R. Granfors. Determination of the modulation transfer function using the edge method: influence of scattered radiation. *Med Phys*, 31(12):3485–3491, Dec 2004.

[22] S. N. Friedman and I. A. Cunningham. A small-signal approach to temporal modulation transfer functions with exposure-rate dependence and its application to fluoroscopic detective quantum efficiency. *Med Phys*, 36(8):3775–3785, Aug 2009.

[23] M.U. Sivananthan A.R. Cowena, A.G. Daviesa. The design and imaging characteristics of dynamic, solid-state, flat-panel x-ray image detectors for digital fluoroscopy and fluorography. *Clinical Radiology*, 63:1073–1085, 2008.

[24] Lyon Industries, 1630 Shanahan Drive, South Elgin, Illinois 60177, www.lyonindustries.com.

[25] M. J. Berger, J. H. Hubbell, S. M. Seltzer, J. Chang, J. S. Coursey, R. Sukumar, and D. S. Zucker. XCOM: Photon cross section database (version 1.3), http://physics.nist.gov/xcom, 2005.

[26] M. C. McDonald, H. K. Kim, J. H. Henry, and I. A. Cunningham. A novel method to measure the zero-frequency DQE of a non-linear imaging system. In N. Pelc and E. Samei, editors, *Medical Imaging 2010: Physics of Medical Imaging*, volume 7961, 2011.

Chapter 3

Conclusions and Future Work

3.1 Conclusions

The motivation of this research is to develop a method to assess the performance and dose efficiency of x-ray imaging systems, irrespective of the system response and processing of the available data. The concept of the neutral-attenuator method was introduced as a means to determine the response of the system and thereby linearize non-linear data and calculate the DQE, even in the presence of adaptive non-linear image-processing. The method was validated on a digital flat panel x ray detector with an adaptive non-linear response which implemented edge-enhancement. The following specific conclusions where made from this work:

1. Using the LSS method, it is possible to measure the DQE using both the raw linear and processed non-linear data to within 5% of a conventional IEC measurement. This is believed to be sufficient for the quality assurance purposes of detecting meaningful changes in system performance, acceptance testing, and evaluating the performance of older equipment for end-of-life decisions making.

2. The image-processing on this system did not increase the DQE. The ability to measure DQE using data that has been undergone extensive processing confirms

that the DQE is a robust measure of performance, and an ideal candidate for the measurement of performance in clinical quality assurance.

In addition, the following observations where made:

1. Gray-scale inversion of the system response, applied by the manufacturer when computing the processed images, did not affect DQE results; and

2. Edge enhancement, applied by the manufacturer to the processed images, affected the MTF and NPS showing an increase in both at mid frequencies, but did not affect the DQE, consistent with expectations for linear processing of image data.

This method solves the problem of measuring the DQE when linear data is unavailable. It is anticipated that this will make DQE measurements more accessible to those without advanced technical knowledge who wish to measure DQE in a clinical setting as part of routine quality assurance.

3.1.1 Limitations

Several limitations of the theory and method presented in this thesis have been identified. These are divided into three categories:

1. Glare and it's effects on the measurement of the system response;

2. Issues pertaining to the use of low-contrast attenuators for test phantoms; and

3. Limitations on the types of image-processing that can be successfully circumvented by this method.

3.1.1.1 Glare

The single biggest limitation on the methods described in this thesis is the glare that is present in some detectors. Glare is due to long-range scattering of x rays and

optical photons and appears as an offset in measured pixel values that is additive to the contribution from theoretical deposited energy. This is a problem because the neutral-attenuator method maps measured pixel values as a function of theoretical deposited energy and therefore does not consider additional offsets such as glare. In Chapter 2 this resulted in an increase in the gain of the system in the linearized system response which was responsible for differences seen in the DQE calculated using LSS and IEC methods. The test system used in this thesis is thought to represents a worst-case scenario for the amount of glare that would be encountered on a digital system.

3.1.1.2 Scatter

The next problem is scatter from low-contrast test objects. Scatter is created by any low-contrast object in the x ray beam, and the effect will be to add to the transmitted x ray beam and impart additional energy to the detector. The low-contrast objects in this study are made of copper, and therefore are subject to this effect. To reduce or eliminate the effects of scatter, measurements using these test objects must be made further from the detector image plane where inverse-square effects reduce scattered radiation. This is effective at reducing scatter but it's not desirable if for instance these methods where to be implemented in a compact test device for easy use in clinical applications due to the space requirements. It is also problematic for the small-signal MTF measurement, because additional effects of distance such as off-axis x rays result in penumbral blur. This limits the range at which the MTF measurement can be made to small distances ($\leq$5 cm), where scatter is still present. Scatter effects on the MTF where further mitigated by employing a smaller window of data for the system edge-response function, however this resulted in a loss of information about the system low-frequency drop.

3.1.1.3 Image-Processing

Finally, the techniques described will not be applicable to all types of image processing. One example of this will likely be certain forms of active noise reduction. In this technique, noise in low-contrast areas that the software perceives as containing uniform intensity x rays will be suppressed by spatial smoothing of pixel values or a similar technique. However, because this algorithm is not applied to noise in high contrast areas of the image where the software perceives an object is present, a DQE test will produce inflated, often nonsensical results [1].

3.2 Future Work

Some suggestions to address the current limitations of the method are now considered. These issues are considered individually in the same as order as the current limitations.

3.2.1 Glare

Optical glare is part of the detector, therefore it is beyond the scope of this work to suggest how it might be eliminated, however there are a number of ways the effects of it might be mitigated. For instance, the fraction of the output measurement contributed by glare is related to the total exposed detector area. For the GE XQ/i Revolution detector used for this thesis, the relationship between the pixel value measured in the centre of the image, and the physical area of the x ray beam on the detector is shown in Fig 3.1. If it is assumed that the increase in pixel value due to an increase in beam area is attributable entirely to glare, then the difference in glare fraction between a very small beam size (approx. 5 cm x 5 cm) and a very large one (40 cm x 40 cm) is of the order 12%, which is quite significant.

Using a smaller size of x ray beam (by collimation) would reduce the glare fraction

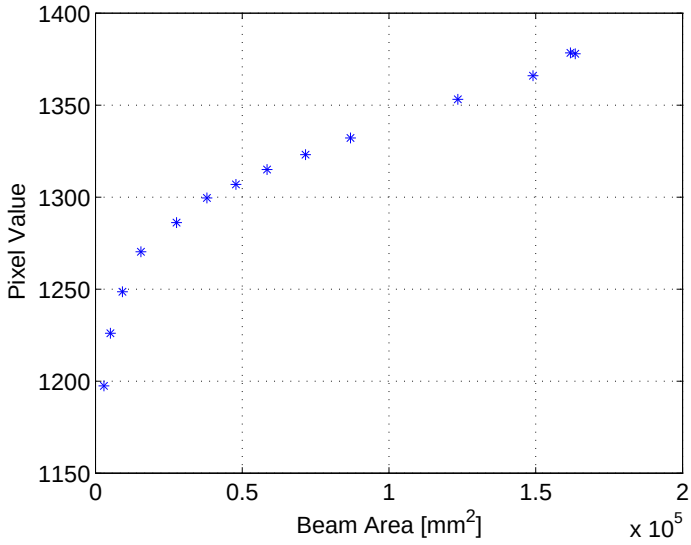

Figure 3.1: Pixel value measured (in image centre) on a GE XQ/i Revolution detector exposed to a IEC RQA-5 spectrum (fixed exposure conditions) as a function of the x ray beam area.

and improve the accuracy. Additionally, it can be seen that the glare is related to the distance of the exposed detector area to the location of pixel value measurement, that is, the contribution from areas further away is lower then the contribution from nearby. Placing attenuators near the edge of the image would maximize the distance over which scattered x ray and optical photons must travel from exposed detector locations, thus minimizing glare.

3.2.2 Scatter

Not a great deal of scatter from low-contrast test objects, other then the measures already taken, such as increasing the distance of the attenuator to the detector, and using different materials for the test objects. One might suppose that a thin sheet of tungsten (K-edge ˜70 keV) would be a good choice of material for the MTF edge due to fewer photoelectric interactions. According to Neitzel [2], a 1 mm tungsten edge will result in less then .1% error in the measured MTF for an RQA-5 which would

be an improvement from the copper edge used in this study, however the relatively high attenuation of this edge ($> 95\%$) may be undesirable in a small-signal method. The scatter performance of any given material as an MTF edge or as a material for mapping of the system response must be evaluated empirically on a case-by-case basis.

3.2.3 Image Processing

For the types of image processing that cannot be easily circumvented with the method, the solution is to attempt to detect the processing and require the user to disable it. Noise reduction for instance could be detected if nonsensical values of DQE, (DQE $>$ 1) are calculated. Although it is counter to the design principle of data agnosticism, this is one case where there is no other viable solution.

Bibliography

[1] H.S. Park, J.H.J. Kim, C. Lee, and Y.N. Coi. Effects of image processing on the detective quantum efficiency. *Journal of Korean physics society*, 56:653–658, 2010.

[2] U. Neitzel, E. Buhr, G. Hilgers, and P. R. Granfors. Determination of the modulation transfer function using the edge method: influence of scattered radiation. *Med Phys*, 31(12):3485–3491, Dec 2004.

Curriculum Vitae

Name:	Michael McDonald
Post-Secondary Education and Degrees:	Western University London, ON 2009 - 2012 MESc. (Biomedical) Western University London, ON 2000 - 2004 BESc. (Electrical)
Related Work Experience:	Research Technician The University of Western Ontario 2008 - 2012 Production Technician Active Control Technology 2005 - 2007

REFEREED JOURNAL PUBLICATIONS

In Preperation:

- M. McDonald, H.Y. Kim, J.Henry, I.Cunningham. *A Method to Measure the Detective Quantum Efficiency in a Clinical Setting.* In preperation for submission to Medical Physics.

CONFERENCE PROCEEDINGS

- M. McDonald, H.Y. Kim, J.Henry, I.Cunningham. A Novel Method to Measure the Zero-Frequency Detective Quantum Efficiency of a Non-Linear X-Ray Imaging System. Society for Photonics and Instrumentation Engineers (SPIE) Proceedings: Medical Imaging 2011.

- M. McDonald, H.Y. Kim, J.Henry, I.Cunningham. *A Novel Method to Measure the Zero-Frequency Detective Quantum Efficiency of a Non-Linear X-Ray Imaging System.* Society for Photonics and Instrumentation Engineers (SPIE) Proceedings: Medical Imaging 2011